NONLINEAR ANALYSIS TECHNIQUES FOR USE IN THE ASSESSMENT OF HIGH-LEVEL WASTE TANK STRUCTURES

Carleton J. Moore[a]
Albert D. Dyrness[b]
Larry J. Julyk[a]
George L. Fox[a]

ABSTRACT

Reinforced concrete in combination with a steel liner has had a wide application to structures containing hazardous material. The buried double-shell waste storage tanks at the U.S. Department of Energy's Hanford Site use this construction method. The generation and potential ignition of combustible gases within the primary tank is postulated to develop beyond-design-basis internal pressure and possible impact loading. The scope of this paper includes the illustration of analysis techniques for the assessment of these beyond-design-basis loadings. The analysis techniques include the coupling of the gas dynamics with the structural response, the treatment of reinforced concrete in regimes of inelastic behavior, and the treatment of geometric nonlinearities. The techniques and software tools presented provide a powerful nonlinear analysis capability for storage tanks.

INTRODUCTION

Reinforced concrete in combination with a steel liner has had wide application to structures containing hazardous material. Radioactive chemical wastes are stored on an interim basis in buried double-shell tanks of similar construction at the U.S. Department of Energy's Hanford Site. The generation of flammable levels of hydrogen gas has been observed in one of the 1,000,000-gal (3,785,000-L) double-shell tanks. An analysis of this tank for a postulated ignition source to investigate the resulting beyond-design-basis pressure loading and possible missile generated impacts was conducted. The use of nonlinear analysis methods were required to adequately assess the structural

[a]Westinghouse Hanford Company, P.O. Box 1970, Richland, Washington 99352.

[b]ADVENT Engineering Services, Inc., 3 Crow Canyon Court, Suite 100, San Ramon, California 94583-1624.

integrity of the tank subjected to extreme loading. The general-purpose finite element program ABAQUS [1] was the chosen analysis tool owing to its versatility in modeling nonlinear problems.

Nonlinearities need to be addressed because of the geometric construction of the tank and the inelastic material response to the extreme dynamic pressure loading due to a postulated ignition of flammable gases. The tank geometry of the 1,000,000-gal (3,785,000-L) double-shell tank is shown in Figure 1. The tank stands about 50 ft (15.2 m) tall with an outer diameter of 88 ft (26.8 m) and a soil overburden of about 6.5 ft (1.98 m) at the dome apex. The reinforced concrete dome is integrally connected to the 3/8-in. (9.5-mm) steel plate (ASTM A516 Grade 65), which form the elliptical head of the primary tank. The primary tank continues down with varying thicknesses as a free-standing vertical wall and closes to form the bottom floor of the primary tank. The secondary tank starts at the tangent point of the primary tank with the steel-lined reinforced concrete haunch and extends down along the concrete wall. The secondary steel liner is attached to the concrete wall by a 2-ft (0.6-m) square pattern of welded anchor studs and separates from the concrete wall at the floor level where it rests but is not integrally connected to the reinforced concrete floor basemat. The concrete wall and basemat are not structurally connected thereby allowing for lift-off separation during rapid pressurization. To allow for lift-off in the finite element model, the introduction of interface elements as shown in Figure 2 was required. Nonlinear stiffness effects were accounted for by the use of large displacement theory, and the potential for sliding friction associated with the side soil/structure interaction was also modeled.

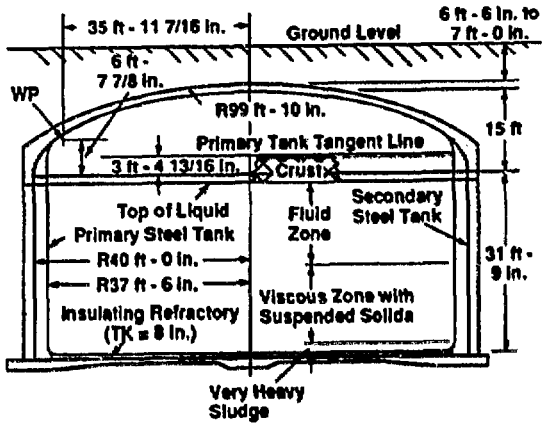

Figure 1. Tank Geometry

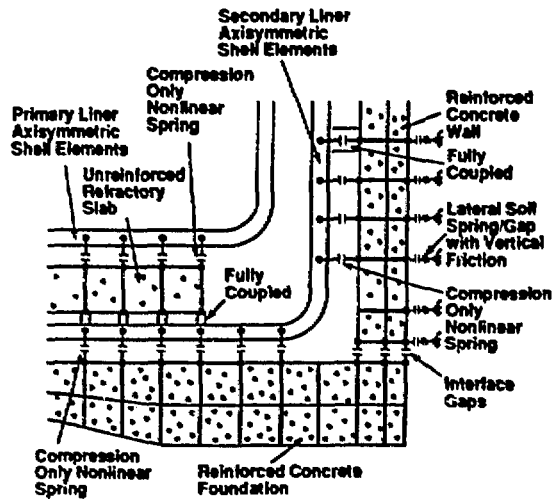

Figure 2. Modeling of the Foundation and Bottom Corner Region

Both the steel liner and rebar plasticity were modeled with an isotropic hardening constitutive model internal to ABAQUS. The rebar is modeled at specific geometric locations within the structure. A smeared-crack reinforced concrete constitutive model determines an element stiffness matrix that accounts for the reinforcement on an integration point basis. The concrete constitutive model addresses pre- and post-crack tension, compressive strain hardening and crushing. The commercially available smeared-crack model, UMAT90 [2], was implemented through a user-defined material subroutine capability available within ABAQUS. Through the use of other user-defined subroutines allowed by the ABAQUS code, DLOAD and UEL were specifically developed for this effort to allow the hydrogen burn model pressure loads to be directly coupled to the structural response.

GEOMETRIC AND BOUNDARY NONLINEARITIES

Many of the classical and finite element structural analysis methods implicitly assume that both displacements and strains developed in the structure are small. This assumption means that the geometry of the elements remains basically unchanged during the loading process and that first order, infinitesimal, linear strain approximations can be used. In extreme load applications, such linear assumptions frequently fail even though actual strains may be small [3]. If an accurate determination of the response of a tank subjected to beyond-design-basis pressure loading is to be made, geometric and material nonlinearities must be considered. The waste tank primary steel liner model must incorporate the stiffness associated with the membrane stresses to properly predict the liner response. This change in structural stiffness as a result of the loading condition is accounted for through large displacement analysis.

Geometric nonlinear dynamic transient analysis also provides a check on potential structural instability phenomena such as classical bifurcation buckling and snap-through buckling. A critical point may be reached where load-carrying capacity decreases with continuing deformation. Large deflection theory addresses the problem of potential structural instability.

However, because the model is axisymmetric, only axisymmetric buckling phenomena are addressed. The tank in this study is of a unique construction consisting of a primary and secondary steel liner with an exterior steel reinforced concrete wall resting on a reinforced concrete basemat (Figures 1 and 2). The outer concrete wall is not connected to the foundation with steel reinforcement. The deflected shape plot of the tank under extreme static pressure is shown in Figure 3. Note that the steel liner bottom tries to assume a hemispherical shape with very little associated liner strain. Large deflection theory is necessary for the proper prediction of this phenomena.

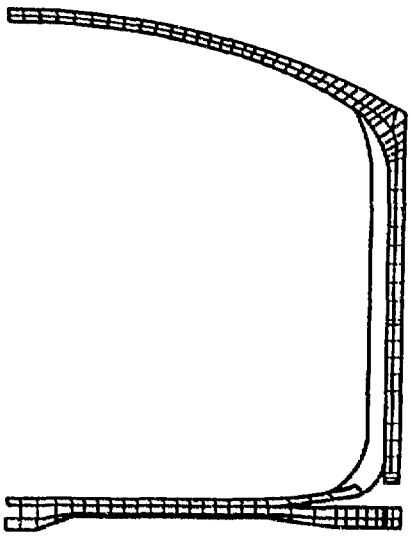

Figure 3. Displaced Shape for Static Internal Gage Pressure of 60 lbf/in^2 without Side Soil Friction.

Another important consideration is the effect of side soil friction, shown in Figure 4 as a function of static internal pressure. Results are depicted with and without friction. Note the dramatic increase in lift-off without friction. Also note that the strain in the dome region is greater with side soil friction. In the case without friction, the strain energy is absorbed over a greater volume of material than is the case with friction.

3.0 NONLINEAR MATERIAL BEHAVIOR

The response of tank structures subjected to extreme loads can force the structural material behavior well into the inelastic regime. The internal pressure loading causes the tank to respond as a tension structure, where the steel liner and concrete reinforcement share the hoop and meridional stresses. There was a clear need to apply a reinforced concrete constitutive model that could remain stable in this regime of significant tensile strain. ABAQUS has an internal reinforced concrete constitutive model developed for relatively monotonic loading, that requires user input of key parameters. The commercially available UMAT90 [2] subroutine sets all other parameters internally to characterize the concrete behavior.

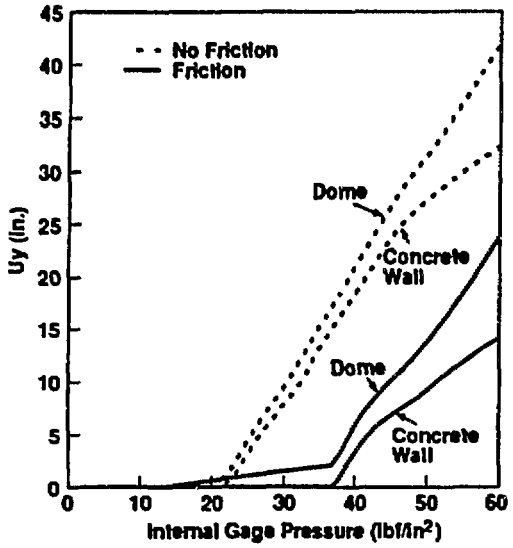

Figure 4. Effects of Side Soil Friction on Static Vertical Displacement of Dome and Concrete Wall.

The shape of the concrete tensile stress-strain diagram is well known, but there is a wide disparity in the literature on the control points. Use of the compressive tangent modulus until the fracture stress (f_t) is reached, as shown in Figure 5, is accepted practice. The fracture stress normally ranges from 5 to 10 percent of the compressive

strength (f_c). Beyond the fracture strain (e_t), the corresponding stress monotonically reduces to zero over a finite strain (e_f). This is known as tension stiffening, which physically represents the transfer of load from the concrete to the rebar over a finite strain. Tension stiffening is characterized by a dimensionless quotient α equal to e_f/e_t that ranges in the literature [4,5] from 2 to 20. A value of 2 corresponds to plain concrete and a value of 20 to heavily reinforced concrete. A similar effect for transferring shear loads is known as shear retention. Shear retention is characterized by the shear retention factor (SRF) defined as the ratio of the strain at which the shear modulus is reduced to zero at the fracture strain.

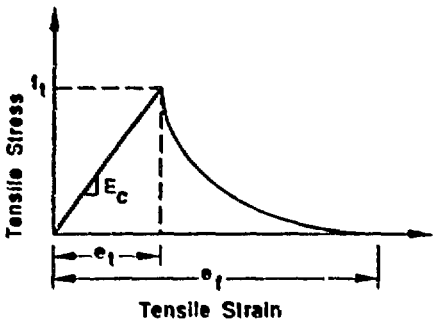

Figure 5. Concrete Tension Stress-Strain Behavior.

The implementation of this nonlinear tensile behavior for reinforced concrete can lead to numerical instabilities [6,7,8]. The instabilities are manifest in a number of ways. Alternate (unstable) equilibrium states can be introduced as a result of tension stiffening [8]. Parallel cracks that occur within an element with little or no shear retention can lead to small pivots, thereby causing numerical instabilities [7]. Residual forces caused by crack initiation can be on the same order as the applied loads, making it difficult for the solution procedure to attain equilibrium convergence. A balance between stability and accuracy of the reinforced concrete material characterization is required. A number of parametric static pressurization cases were performed to investigate the effects of the key parameters of the constitutive model on the structural response. Eight cases were evaluated: five using the ABAQUS constitutive model, two using UMAT90, and one that excluded the concrete completely.

Table 1 contains the parameters that were varied. The strain at a global discontinuity was plotted for each case as a function of static gage pressure in Figure 6. The steel-only case provided a well-behaved solution with a tensile strain exceeding 6 percent at an internal gauge pressure of 60 lbf/in^2. From these results it is clear that the reinforced concrete significantly increases the stiffness of the structure until significant cracking has been achieved. Beyond a gauge pressure of about 40 lbf/in^2, the stiffness for cases with concrete explicitly modeled is close to the stiffness observed. The UMAT90 and the ABAQUS models gave similar results, providing independent verification of the reinforced concrete constitutive models. The variation in tension stiffening and shear retention for the range investigated did not significantly affect the solution accuracy. However, numerical stability was

affected by low values of tension stiffening and shear retention. To avoid numerical instabilities caused by the rapid change in stiffness associated with concrete cracking, the second linear relation of the Cope [5] bi-linear curve was extended to represent the entire post-fracture stress-strain diagram as illustrated in Figure 7. Because UMAT90 was more suited for cyclic behavior and used material damping on an integration point basis, it was chosen for the dynamic analyses.

Case No.	Acronym	β	α	SRF
1	abqst	NA	NA	NA
2	umt	0.1000	2	40.0*
3	umtnt	0.0100	2	40.0*
4	abq	0.0722	10	∞
5	abqlts	0.0500	10	∞
6	abqnsr	0.0722	10	0.0
7	abqlsr	0.0722	10	1.1
8	abqmsr	0.0722	10	11.0

β = Ratio of the uniaxial tensile to the uniaxial compressive strength (f_t/f_c).
α = Ratio of the fracture strain to the tensile strain at zero stress (e_t/e_f).
SRF = Shear retention factor, ratio of the strain at which the shear modulus is reduced to zero to the fracture strain.

*SRF is calculated at the strain that reduces the shear modulus to 1 percent of the uncracked value.

Table 1. Concrete Parameters Used in Comparative Study

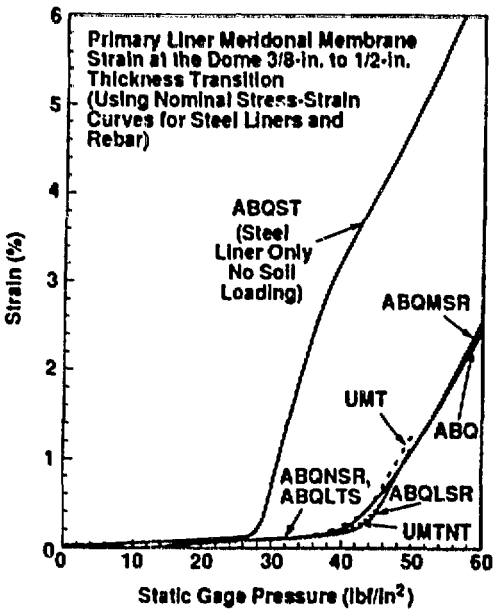

Figure 6. Concrete Material Model Comparison of Eight Cases

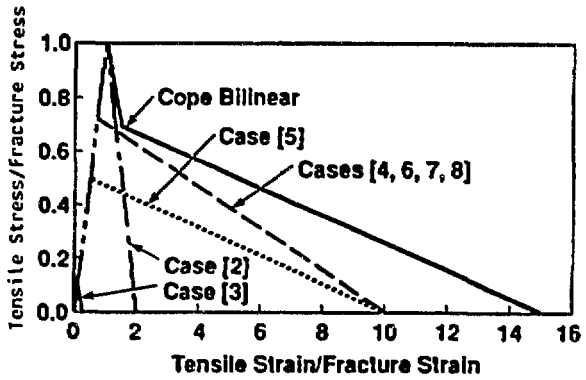

Figure 7. Tensile Behavior

DYNAMIC PRESSURE AND IMPACT LOADING WITH STRUCTURAL INTERACTION

The surface of the tank waste is covered with a crust that has been known to slowly rise over a period of 6 to 16 weeks, vent gas, and drop back approximately to its original level. The postulated

hydrogen burn loads the structure via an internal pressure. The internal pressure is calculated based on a thermodynamic quasi-equilibrium state. The ideal gas law is applied at each time step. Therefore, a scheme was developed to calculate the volume change interactively as a function of time and use this instantaneous volume to determine the equilibrium pressure. This interaction is done for the gas within the primary tank liner, as well as for the air within the secondary tank liner annulus cavity.

The thermodynamic equilibrium calculations are performed in a user-defined distributed load subroutine (DLOAD) that applies the pressure to all of the elements. The volume is calculated in a user-defined UEL element subroutine [1]. The user-defined element is a dummy element. It is defined with all of the nodes in the primary liner and the secondary tank liner nodes bounding the annulus cavity. The UEL subroutine can communicate the nodal displacements calculated from ABAQUS as required to calculate the volume changes. A Fortran common block in both the UEL and DLOAD subroutines allows communication of the time-dependent volumes.

The pressure calculations performed in the user DLOAD subroutine are performed one time step behind the structural solution to avoid additional solution iterations. The time steps in the dynamic analyses are quite small, on the order of 0.0001 s. Therefore, the error is well within the accuracy of the analysis goals.

HYDROGEN DOME BURN CHARACTERIZATION

The gas dynamics of the dome burn case were modeled as follows. A hydrogen and N_2O gas mixture was assumed to exist in the waste. The hydrogen gas mix is assumed to vent into the dome area and mix with an oxygen and nitrogen mixture. Ignition is assumed with an axisymmetric flame propagation. The pressures behind and in front of the flame front are assumed to be the same. The burn gases are assumed to form a bubble of gas at a uniform pressure and temperature. This simplified thermodynamic gas burn model does not consider wave or shock propagation.

Energy Release

The hydrogen gas release has the potential of burning with N_2O below the crust or with both N_2O and oxygen in the tank dome, although a burn below the crust is considered highly unlikely. The energy release for both reactions is as follows.

The burning of hydrogen with N_2O is represented by the following stoichiometric equation:

$$H_2 + N_2O \rightarrow H_2O + N_2. \qquad (1)$$

For hydrogen-oxygen mixtures, combustion is represented by

$$H_2 + \frac{1}{2}O_2 \rightarrow H_2O. \qquad (2)$$

The heat of combustion is computed by adding heats of formation.

Thermodynamic Burn Model

This model uses thermodynamic relationships to calculate

pressure and temperatures from the heat of combustion for hydrogen and N_2O mixtures. The following thermodynamic burn model was employed for the burn above the crust, as well as below the crust. The equations follow directly from the first law of thermodynamics for a closed system as shown in Equation 3.

$$dU = dQ - dW \qquad (3)$$

where

U = System internal energy
Q = Summation of heat terms
= heat of combustion
W = Summation of work terms

The specific heats must be calculated as a function of temperature. Correlations have been used for temperature-dependence over the temperature range 32 °F to 6,400 °F [9].

The system work energy is rewritten as

$$dW = PdV = PV\frac{dV}{V} = m(h-u)\frac{dV}{V} \qquad (4)$$

where

h = Specific enthalpy (per mole)
u = Specific internal energy (per mole)
V = System volume
P = Pressure.

Combining Equation 4 with Equation 3 and solving for the rate of temperature change for an ideal gas produces

$$\dot{T} = \frac{\dot{Q}}{mC_v} - \frac{(h-u)}{C_v}\frac{\dot{V}}{V} \qquad (5)$$

where $(\cdot)$ signifies a derivative with respect to time. The gas law may be used to obtain a relationship for pressure rate change, that is

$$\dot{P} = P\left[\frac{\dot{T}}{T} - \frac{\dot{V}}{V}\right]. \qquad (6)$$

Equation 5 and the system work done by the change in volume complete the thermodynamic equations necessary to define the system. However, the two rate terms of Equation 5 must be obtained from system responses. For example, the volume expansion term is dependent on crust and wall motion. The heat term is based on a burning model that uses a constant velocity flame front moving from the center of the tank to the vessel wall. The heat input rate is then proportional to the velocity and flame front circumference. Hence, the burn time is an input parameter.

The nonlinear dynamic response of the structure is captured in Figures 8 and 9 where the phasing between the loading (pressure) and response (volume change) are illustrated. In fact, when pressure loading is plotted against change in volume, the time parameter drops out as shown in Figure 10. The area under the pressure-versus-volume plot is a measure of the strain energy and kinetic energy absorbed by the structure and provides a means to develop equivalent static

pressures for dynamic loading. It also reduces a multi-degree of freedom model to an intuitive single degree of freedom.

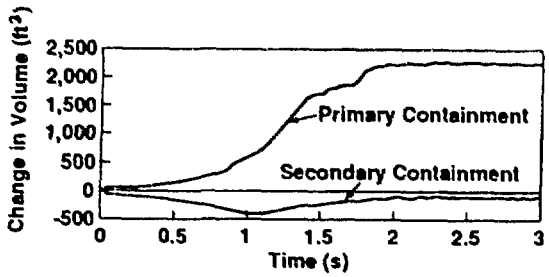

Figure 8. Best-Estimate Volume Change History for the 1-s, 4,200 ft^3 Burn Above Crust with Side Wall Friction.

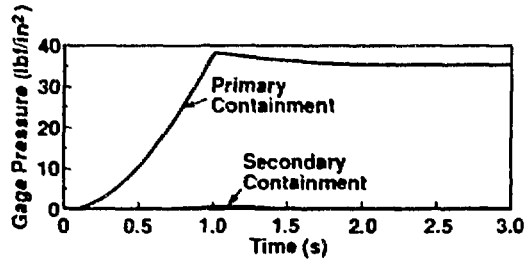

Figure 9. Best-Estimate Pressure Loading History for the 1-s, 4,200 ft^3 Burn Above Crust with Side Wall Friction

Axisymmetric UEL Volume Calculation

The axisymmetric volumes of the primary tank liner, secondary tank liner, and the volume under the moving crust were calculated by a user-defined element subroutine. ABAQUS has the capability to input an element subroutine called UEL. The user-defined UEL subroutine was programmed in Fortran to calculate the axisymmetric volume of the element, but the subroutine does not add any structural stiffness to the system.

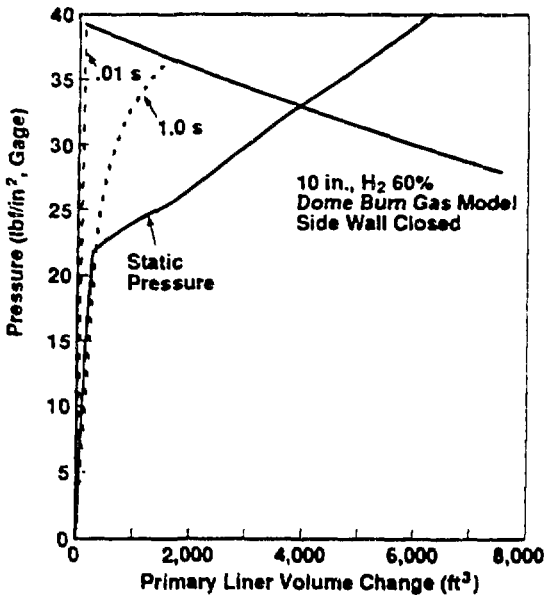

Figure 10. Pressure - Volume Diagram for Dynamic 1-s, 10 ms and Static Cases, without Side Soil Friction.

The ABAQUS UEL subroutine has array variables that include the original geometry of the element nodes and the current estimated nodal displacements, velocities, and accelerations. The original geometry and the displacements in the radial and vertical directions are used to calculate the axisymmetric volume enclosed by the element nodes. The axisymmetric volume between two nodes is assumed to be a slice of a cone, and the slices are added proceeding from bottom to top (Figure 11). The relation for the volume of a slice of cone is as follows [10].

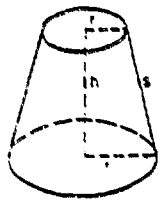

Figure 11. Volume of a Cone Slice.

$$V = \frac{1}{3}\pi r^2 h[1 + (r'/r) + (r'/r)^2] \quad (7)$$

The volume history calculations provide insight to the structural behavior. Figure 8 shows the volume history of both the primary and secondary containment for a 1-s, 4,200 ft^3 (119 m^3) burn above the crust.

IMPACT LOAD CHARACTERIZATION

The investigation of the transient response of the tank to a postulated ignition included an ignition of a 50 percent hydrogen and 50 percent N_2O gas mix under the crust that represents the most energetic ignition. A burn under the crust would accelerate the crust upward until it impacts the dome.

ABAQUS Crust Impacting Model

The structural characteristics of the crust were originally modeled with axisymmetric solid elements. The solid elements forming the crust are not connected and are assumed to be frictionless nested rings. The finite element mesh of the crust matches the distribution of nodes in the dome of the tank primary liner. The crust nodes were constrained to allow only vertical translation. The crust elements are loaded on the top and bottom faces by gas pressures developed in a special user-defined DLOAD subroutine. Gap elements are defined between the crust and the dome to model impacting. No gas leakage is assumed between volumes, i.e., above and below the crust. In addition the trapped air above the crust is compressed because no venting of gas out of the tank is assumed.

The ABAQUS simulation of the impacting event with the crust explicitly modeled is numerically intensive. ABAQUS required very small time steps to achieve convergence. The crust was modeled as an elastic/perfectly plastic material. The elastic modulus was set at the value used for concrete, and the yield stress was set at 100 lbf/in^2 to simulate the crust.

The model has three gas volumes that respond to the structural deflections and load the surrounding elements. The first gas volume is the burning gas assumed to be under the crust; the second is trapped air between the secondary and primary liners. The third gas volume is the air trapped in the dome above the rising crust. The first gas volume employs the simplified thermodynamic gas model as previously discussed. The latter two obey the adiabatic gas relations for air. Volume calculations made under the crust incorporate the rising of the crust as it responds to pressure. These calculations have logic to sense the height of the crust. Figure 12 shows the volume history of the primary and secondary tank liners. Note that spikes

associated with crust impact loads are evident. Figure 13 shows the time progression of the crust elements impacting the dome at 1.5 s for a 1-s, 4,200 ft^3 (119 m^3) below-crust burn.

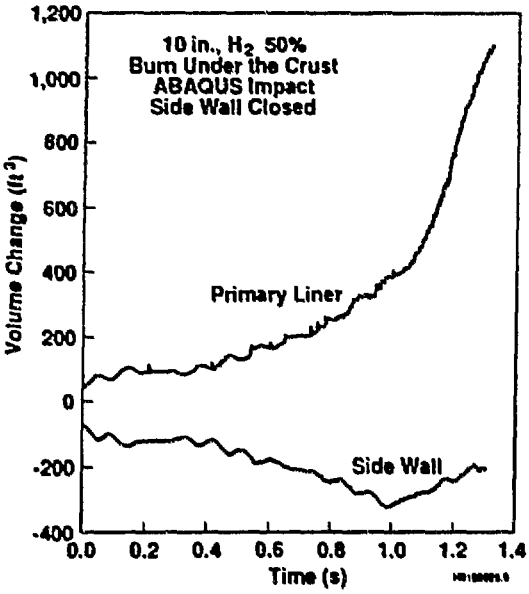

Figure 12. Comparative Volume Change History for 1-s, 4,200 ft^3 Burn Below Crust without Side Soil Friction.

Simplified ABAQUS Crust Impacting Model

It is considered more probable that the crust would break up on initial impact with the dome at the outer edge of the crust. This crust breakup would allow the pressure to equalize and the gas below and above the crust to mix. Hence, the subsequent burn would behave more like a burn in the dome with the associated pressurization but with impacts from the crust.

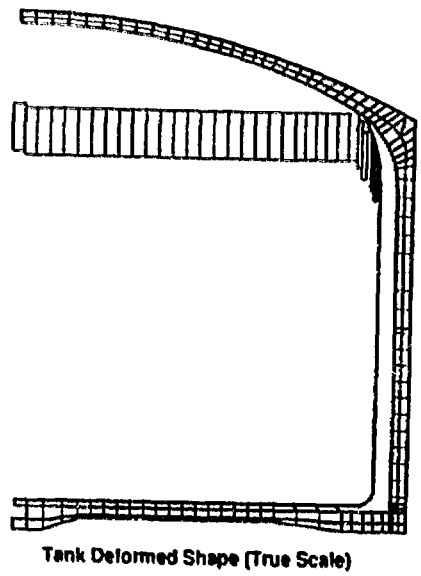

Figure 13. Cascading Impacts on Tank Dome at 0.3, 0.6 and 0.8 s for 1-s, 4,200 ft^3 Burn Below Crust with Impacting Crust.

The simplified ABAQUS crust-impacting model employed the burn in the dome gas model with impacts defined by pressure sine pulses. Sine pressure impulses were defined in a special-purpose user-defined DLOAD subroutine. The initial contact time and initial velocity of the crust when the crust first contacts the other edge of the dome was obtained from previous results from both the ABAQUS model and with a simplified thermomechanical model developed on a personal computer.

Momentum was assumed to be transferred with no elastic rebound. The shape of the pressure pulse was assumed to be sinusoidal with a duration of one-half the period.

Hence,

$$mv = \int_o^{t_d} F(t)\,dt = \int_o^{t_d} F_p \sin\left(\frac{\pi t}{t_d}\right) dt \qquad (8)$$

where

F_p = Peak load
t_d = Impulse duration.

The resulting pressure sine impulse is given by

$$P(t) = \frac{mv\pi}{2At_d} \sin\left(\frac{\pi t}{t_d}\right) \qquad (9)$$

where

A = Area of shell element impacted
P(t) = Pressure as a function of time.

The above assumes that the crust material experiences a plastic impact and the resulting load acts perpendicular to the dome element area being impacted.

CONCLUSIONS

Demonstrations of nonlinear techniques have been illustrated that are useful in assessing the integrity of tank structures. The effect of large displacement theory in problems involving lift-off, stress-stiffening, or structural instability should not be neglected. The capacity of the tank was substantially increased by the application of large displacement theory. The effect of side soil friction significantly altered the structural response. The inclusion of side soil friction for buried tanks will not always be conservative. The tank will experience greater uplift for the frictionless model, but the hoop stresses will be significantly increased for the model with friction. It was also demonstrated that the structural response of reinforced concrete is highly nonlinear and can be modeled with a high degree of precision by invoking commercially available subroutines linkable to ABAQUS. An alternate calculation of the concrete treatment can be easily accomplished by using the ABAQUS internal constitutive model in a parallel analysis. Other user-defined subroutines accessible in ABAQUS allow the direct coupling of dynamic impact and pressure loading with the structural response. This feature is especially important when the driving force is pressure developed from a chemical reaction and advantage can be taken from significant changes in the control volume. Utilizing the change in volume allows very complex nonlinear dynamic problems to be simplified to a single variable that can be readily understood. The combination of the nonlinear techniques employed in the analysis of the buried double-shell waste tank provide formidable tools for assessing the integrity of structures subject to extreme loads.

REFERENCES

[1] Hibbitt, Karlsson & Sorensen, Inc., ABAQUS User's Manual, Version 4.8, Providence, Rhode Island, 1989.

[2] ANACAP-U, ANATECH Concrete Analysis Package Version 90-1.0, User's Manual, ANATECH Research Corporation, La Jolla, California, August 1990.

[3] O. C. Zienkiewicz, The Finite Element Method, McGraw-Hill Book Company, New York, New York, 1977.

[4] R. J. Cope, "Material Modeling of Real Reinforced Concrete Slabs," Proceedings of the International Conference of Computer-Aided Analysis and Design of Concrete Structures Part I, edited by F. Damjanic et al., Pineridge Press, Swanson, U.K., 1984, pp. 85-117.

[5] W. C. Schnobrich, "The Role of Finite Element Analysis of Reinforced Concrete Structures," Finite Element Analysis of Concrete Structures, American Society of Civil Engineers, New York, New York, 1990, pp. 1-23.

[6] M. A. Cristfield, "Difficulties with Current Numerical Models for Reinforced Concrete and Some Tentative Solutions," Computer Aided Analysis and Design of Concrete Structures, Part I, edited by F. Damjanic et al., Pineridge Press, Swanson, U.K., 1984, pp. 331-357.

[7] F. Gonzalez-Vidsosa et al., "On the Numerical Instabilities of the Smeared Crack Approach in the Non Linear Modeling of Concrete Structures," Communications in Applied Numerical Methods, 4, 1988, pp. 799-806.

[8] M. A. Cristfield, "Snap-Through and Snap-Back Response in Concrete Structures and the Dangers of Under Integration," International Journal for Numerical Methods in Engineering, Vol. 22, 1986, pp. 751-767.

[9] O. A. Hougen, K. M. Watson, and R. A. Ragatz, Chemical Principles, Part II, Thermodynamics, 2nd Edition, John Wiley & Sons, New York, New York, 1959.

[10] Mark's Standard Handbook for Mechanical Engineers, 7th Edition, Editor Theodore Baumeister, McGraw-Hill, New York, New York, 1967, pp. 2-20.